

Characteristics of a Ce-Doped silica fiber irradiated by 74 MeV protons

N. Savard^{a,b}, D. Potkins^c, J. Beaudry^d, A. Jirasek^b, C. Duzenli^d, C. Hoehr^{a,*}

^a TRIUMF, Vancouver, BC, V6T 2A3, Canada

^b University of British Columbia-Okanagan, Kelowna, BC, V1V 1V7, Canada

^c D-PACE, Nelson, BC, V1L 4B6, Canada

^d British Columbia Cancer Agency, Vancouver, BC, V5Z 4E6, Canada



ARTICLE INFO

Keywords:

Proton therapy
Dosimetry
Inorganic scintillator
Quenching

ABSTRACT

A Ce-doped silica fiber, part of the UniBeAM25 charged-particle beam profiler system from D-Pace, was tested for use in proton therapy dosimetry with a 74 MeV proton beam at the Proton Therapy Facility at TRIUMF, Canada. Repeatability, dose response, dose rate response, and measurements of the horizontal, vertical and axial beam profiles for a raw Bragg peak as well as a spread-out Bragg peak were investigated. For the given irradiation conditions, the fiber's light output was reproducible with percent standard deviation of 1.15%, and has a linear response to irradiated dose length, accumulated dose, and total dose rate with $R^2 > 0.99$ for each. A significant quenching of the signal at high energy deposition for protons was observed, with a peak-to-plateau value of 2.79 and a Birk's constant of $k_B = 2.34 \times 10^{-2} \text{ cm/MeV}$.

1. Introduction

Scientists working in radiation therapy have a need for detectors which can offer high-resolution measurements of relative beam dose within some depth of tissue-equivalent material. Rare-earth doped silica fibers may have potential for ionizing radiation measurements due to their small size and therefore higher spatial resolution, fast fluorescent decay time (Vedda et al., 2004) for real-time measurements, and radiation hardness compared to organic scintillators (Yanagida, 2013).

Doped fibers operate through the process of scintillation, in which charged-particle beams deposit their energy into the fiber material by ionizing bound electrons, which can then combine with activators (or dopants) within the material to create metastable (higher energy, low lifetime) atomic states. Consequently, these atoms relax back into the ground state through the emission of fluorescent light. Scintillators are usually chosen so that the photons produced are within the visible range of light, and therefore can be transported through optical fibers to a photodetector, which outputs a current proportional to the deposited energy of the irradiating particles. The fluorescence light emission within a scintillator is proportional to the particles stopping power via the Craun-Birks equation (Knoll):

$$\frac{dL}{dx} = \frac{S \frac{dE}{dx}}{1 + k_B \frac{dE}{dx} + C \left(\frac{dE}{dx} \right)^2} \quad (1)$$

where E is the energy deposited by the particle, x is the distance

traversed by the particle, L is the emitted fluorescence energy, S is the scintillation efficiency, k_B is Birk's constant which accounts for quenching of the scintillator at higher stopping powers, and C an additional fitting parameter used to better model the scintillator's light output.

Cerium doped silica scintillators have been tested with photon, electron, and proton beams in various capacities before (Vedda et al., 2004; Mones et al., 2006; Veronese et al., 2010). These scintillators tend to have a desired linear response to irradiated dose and dose rate with coefficients of determination $R^2 \approx 1$. The greatest issue with these fiber detectors remains to be the quenching at high energy deposition (large k_B factor) of the particles within the fiber. Quenching is when a large portion of the deposited energy in a scintillator is no longer used in production of fluorescent light, but rather in other processes such as heat (Knoll).

In this paper, we are testing a cerium doped scintillator which is used as part of the UniBeAM beam profiler system from D-Pace Inc., which is currently sold commercially for the purposes of beamline steering and focusing optimization in charged-particle accelerators. The purpose is to measure the characteristics of this fiber under irradiation of protons used for proton therapy, and therefore determine if such a fiber could also be used effectively within the field of dosimetry.

2. Materials and methods

The detector we are using is part of the UniBeAM25 system licensed

* Corresponding author.

E-mail address: choehr@triumf.ca (C. Hoehr).

by D-Pace (UNIBEAM25) from AEC-LHEP University of Bern. The UniBEaM includes the following components: A 29 mm long, unclad 200 μm diameter Ce-doped silica fiber (Braccini et al., 2012) is connected by a commercial fiber (400 μm diameter, 0.5 NA, PVC sheathed from Thorlabs, model FP400URT) to a Silicon Photo-multiplier (SiPM, Sensl C-series) which produces a current proportional to the incident light. This current is read by an ORTEC 439 Digital Current Integrator, which essentially integrates the current over some given time and outputs a proportional number of counts, and is then recorded by the TRIUMF Proton Therapy acquisition system.

The proton beam is continuous with an initial energy of 74 MeV, and operates at currents of 6 nA (DC), though the range can be varied between 1 and 10 nA. The dose provided by the beam is controlled via a transmission chamber just upstream of the beam nozzle, which measures dosage in Monitor Units. For measurements and calibration purposes, detectors can be mounted on a 3D stage which is set up to take transverse and axial scans with respect to the incoming proton beam within a water box. The beam penetrates the water box through a thin (≈ 1 mm) water-equivalent window.

The fiber was attached to a translation apparatus, which can move the water-immersed fiber in three dimensions along the axis of the box with a resolution limited to 0.2 mm. The uncertainty in position along any direction is estimated to be ± 0.1 mm. The fiber was placed with its axis perpendicular to the proton beam trajectory. The detector is moved in set step sizes, and at each step the fiber remains stationary for the time it takes to accumulate the set dose as measured by the transmission chamber. Unless otherwise stated, the dose accumulation at each point was 5000 MU. Due to the time it takes for the beam to shut off, the transmission detector will have readings slightly higher than the set dose. Therefore, to correct for this effect, it is standard to divide the counts over the MU reading. Collimators were placed at the end of the beamline right before the water phantom to collimate the beam to small transverse sizes (≤ 25 mm) so that only the scintillating fiber was irradiated. Collimator openings were either round or square. A simplified schematic with the water box, translation apparatus, and beamline is shown in Fig. 1. Measurements were taken with all lights in the room switched off to minimize ambient light collection.

As the proton beam penetrates the water box at increasing depths, there is an increase in deposited dose until a peak is reached at approximately 3.5–4 cm, which is commonly called the Raw Bragg Peak (RBP, see Fig. 9). This is the result of the increase in energy loss per path length, $\frac{dE}{dx}$, of the protons as they loose energy to the water.

As the RBP is too narrow for treatment of typical tumors, the beam needs to be spread out. For this purpose, a modulator wheel can be mounted at the front of the beam line with different thicknesses at different angles about its center. The wheel's thickness increases as a

function of angle, which means a particle going through different angular sections of the wheel will have different output energies. The wheel is put in front of the beam, and is rotated to change the beam's energy, which changes the distance it can penetrate inside the water. Thus a Spread Out Bragg Peak (SOBP) is created, which is essentially a superposition of depth-dose profiles of different initial energies to create a long plateau (in depth) of constant dose deposition (see Fig. 10). The modulator wheel used here creates a plateau length of about 23 mm within the water. Measurements taken in the so-called reference condition are made with the fiber axially placed along the plateau region of the 23 mm SOBP, while centered horizontally and vertically in the proton's transverse plane. In reference conditions, $1 \text{ MU} = 1.41 \times 10^{-4} \text{ Gy}$ in water.

Measurements taken in the water phantom are used to investigate the reproducibility of the fiber detector, its dose response by taking longer measurements at constant dose rate, and the dose rate response for varying beam currents. Its response as a function of irradiated fiber length is assessed by taking horizontal and vertical beam profiles. Energy dependence and quenching is measured via depth dose profiles.

A Monte-Carlo simulation was performed with SRIM-2013 (Ziegler) which simulates the interactions of charged particles as they traverse matter. Following from Torrisi (2000), we obtained the expected proton energy loss due to ionization as a function of depth in water.

3. Results and discussion

3.1. Scintillator repeatability

Repeated horizontal scans were made with the fiber at the reference position within the plateau of the SOBP. Ten horizontal scans were completed using a 15.4 mm square collimator. For each scan, the three points in the middle of the horizontal plateau were used, generating 30 total points in total. At all positions, the detector signal was normalized to the dose recorded by the transmission detector. At each point, data was taken for about 3 s. The background signal from the fiber and SiPM, given by this signal when positioned outside of the beam, is subtracted off for all scans, and is the case for all scan measurements unless explicitly stated. The percent standard deviation ($\frac{\sigma_A}{A}$) was found to be 1.15% among the points, with the mean counts/MU being 0.0319. This is a bit larger than the $\approx 0.5\%$ seen using similar fibers irradiated with photons and protons (Veronese et al., 2010; Mones et al., 2008), though the reproducibility is dependent on the stability of the entire system (proton beam, SiPM, Transmission Detector, etc) as well.

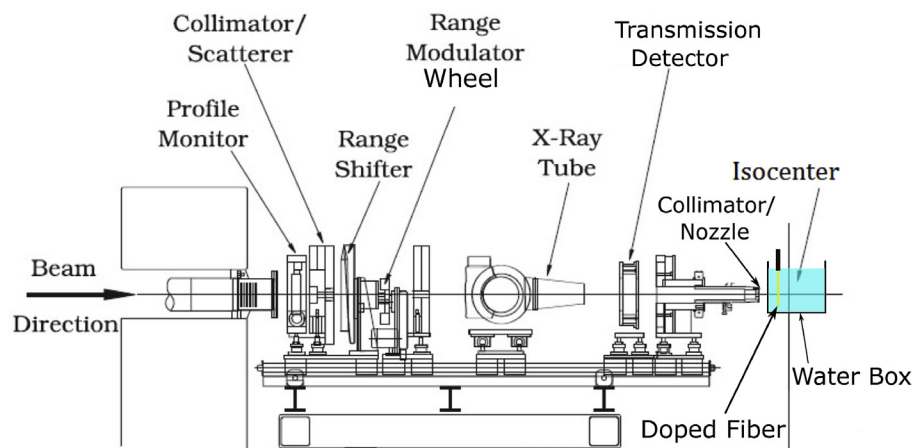


Fig. 1. Side view of beamline used in these experiments. Shows the transmission detector, the modulator wheel, the nozzle/collimator, water box, and an example of how the fiber sits in the water box.

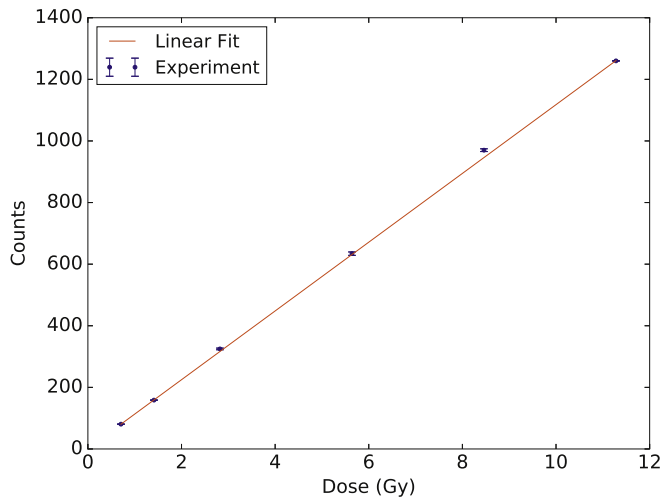


Fig. 2. Integrated counts as a function of set dose for the fiber. Measurements taken within the SOBP plateau at a depth of 20.6 mm in water. Linear regression has $R^2 > 0.99$. The slope is 111.6 ± 0.1 counts/Gy, the intercept is 1.6 ± 0.4 counts.

3.2. Scintillator dose response

To measure the scintillators response to varying accumulated dosage, the horizontal scans in the SOBP were repeated (with 15.4 mm square collimator) while varying the set dosage from 0.705 to 11.28 Gy (5000–80,000 MU). Fig. 2 shows the results of this experiment. The response of the fiber is linear to the varying dose of the proton beam, with $R^2 > 0.99$.

At a depth of 0 mm within the water box and with the 23 mm modulation wheel, we measured horizontal profiles for square collimator sizes of 5.15 mm, 8 mm, and 15.4 mm widths and 5000 MU per step. It should be noted that the 0 mm depth point for the fiber is when it is as close to the edge of the box, and therefore to the beam collimator/nozzle, as possible. The fiber cannot be directly flush against the edge due to the physical size of the attached optical fiber. The plateau of the profile was measured by finding the points which represent $0.9 \times$ peak value or greater, and then averaging the middle 50% of those values. The plateau values are linear with collimator size (see Fig. 3, $R^2 > 0.99$), implying that the fiber response is proportional to the length of irradiated fiber as expected.

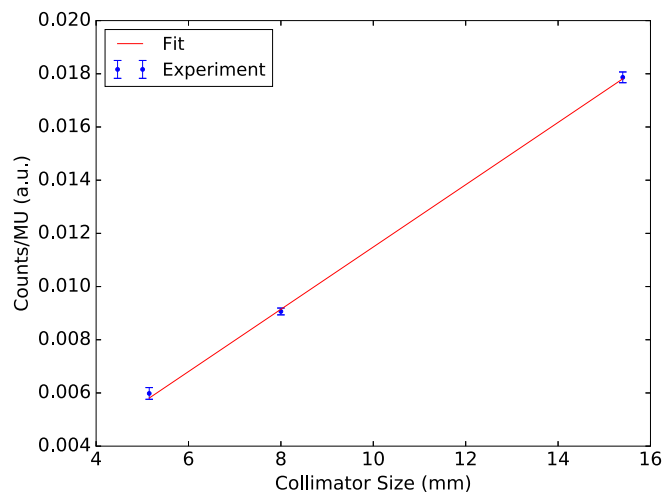


Fig. 3. Signal from fiber as a function of its irradiation length. Taken at depths of 0 mm. Linear regression has $R^2 > 0.99$. The slope is 0.00117 ± 0.00003 , the intercept is -0.0002 ± 0.0003 .

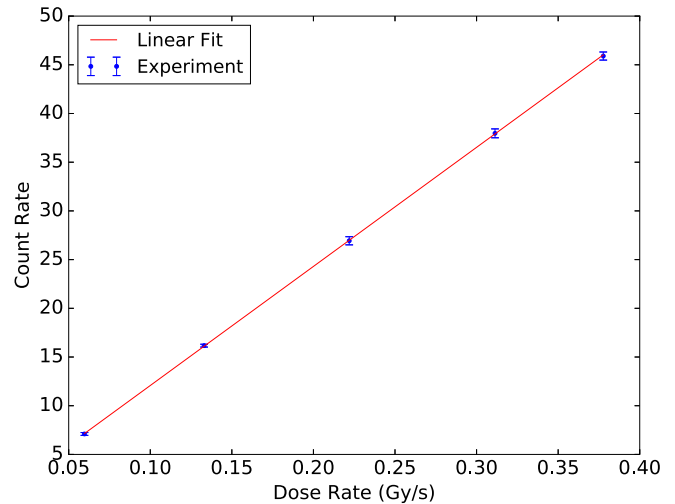


Fig. 4. Count rate from the fiber as a function of dose rate. Measurements taken within the SOBP plateau at a depth of 20.6 mm in water. Linear regression has $R^2 > 0.99$. The slope is 122 ± 1 , the intercept is -0.2 ± 0.2 counts.

3.3. Scintillator dose rate response

We also performed horizontal scans with a 15.4 mm square collimator within the plateau of the SOBP, where the set dosage at each stepping point was constant at 5000 MU, but changed the beam current in order to observe the signal count rate as a function of dose rate, see Fig. 4. The response of the fiber is linear to the varying dose rate of the proton beam, with an $R^2 > 0.99$.

To investigate the effect of different proton energies on the dose rate dependence, we repeated these measurements at different depths in the water phantom without the modulator wheel, essentially sampling different points along the RBP. The depths were at 4.0 mm, 15.9 mm, and 31.7 mm. At each depth, the current of the beam, and therefore dose rate, was varied at approximately 2, 4, 6, and 8 nA. The signal rate as a function of the recorded dose rate (proportional to current) is plotted for each depth in Fig. 5, along with the corresponding linear fits.

At all depths, the linear regressions had $R^2 > 0.99$, and so regardless of the energy deposited within the fiber, the count rate remains linear with current and therefore dose rate. It appears the quenching effect does not affect the fibers linear response to beam current and therefore dose rate, meaning measurements at constant depths in water

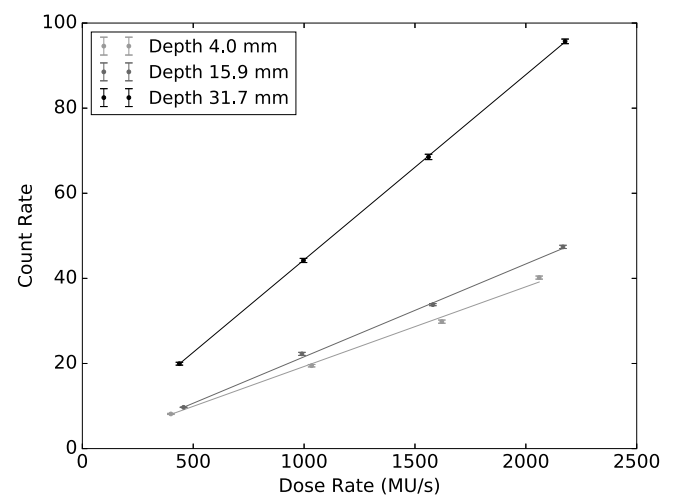


Fig. 5. Dose rate response at depths of 4.0, 15.9, and 31.7 mm in the water phantom. All linear regressions have $R^2 > 0.99$. The intercepts are 0.6 ± 0.2 , -0.3 ± 0.1 , and 0.9 ± 0.4 , respectively.

can be taken without correction for this effect. There is, however, an effect due to increasing proton energy deposition, $\frac{dE}{dx}$, at increasing depths which results in greater fluorescent light emission (see Eq. (1)). This results in an increase of counts from the SiPM, which means the slopes will also increase proportionally to this light output at each depth. The slopes of each linear curve are 0.0187 ± 0.0002 , 0.0218 ± 0.0002 , and 0.0435 ± 0.0003 counts/coulomb at depths of 4.0 mm, 15.9 mm, and 31.7 mm respectively. The ratio of slopes of the last two depths over that at 4.0 mm is 1.16 and 2.32 respectively, which are the sort of ratios we expect from the RBP (see Section 3.6).

3.4. Horizontal profiles

Horizontal scans were taken with 0.8 mm step sizes without any water in the box (at 0 mm depth) using a circular collimator of 25 mm diameter for the beam. The counts at each position is divided by the MU measured by the transmission detector at that position. The profile of the beam, with the peak normalized to 1, should be:

$$y = \frac{1}{A} \sqrt{A^2 - (x - B)^2} \tag{2}$$

with A the radius of the beam, x the horizontal position, y the normalized counts of the beam, and B the center position of the beam. This assumes the fiber's response is linear to its irradiated length.

The profile is shown in Fig. 6, along with a fit to the expected profile for a cylindrical beam. We see that the beam diameter extends about 26.2 mm according to the fit, and so the beam diverges slightly, and may be additionally scattered by the entrance to the water box. It is also possible the fiber was at a slight angle in the transverse plane of the beam since we placed the fiber by eye, which would also result in a slightly broadened profile.

Horizontal scans were taken with 0.5 mm step sizes using a square 15.4 mm collimator at three depth positions within the water: near the entrance of the water boundary, near the half-maximum dose point, and near peak dose to see how the beam diverges within the water. An example raw plot of the horizontal profile at 29.0 mm depth is given in Fig. 7. The information is given in Table 1, with the FWHM (full-width half-maximum), as well as the 10%–90% penumbra width (PW9010, averaged for both sides) being determined through linear extrapolation between the nearest data points. The transverse spread of the beam, represented by the PW9010, at different depths in water is due to proton scattering, though the FWHM does not vary much.

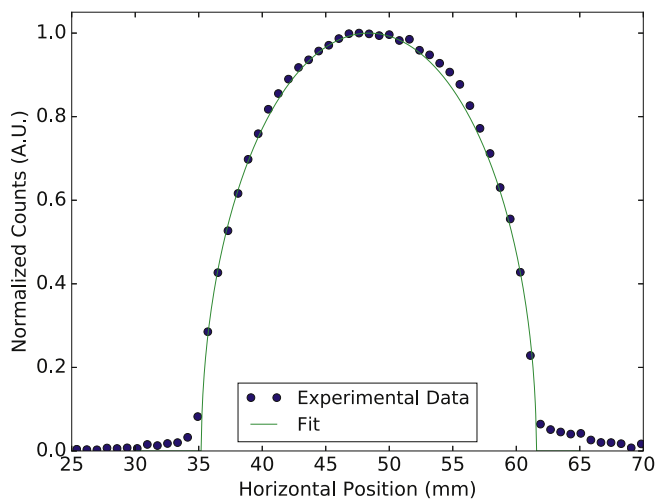


Fig. 6. Horizontal proton beam profile of a 74 MeV proton beam in air using a 25 mm diameter circular collimator (dots), and fit for a circular beam corresponding to a 26.2 mm diameter. Both curves are normalized to their peak values.

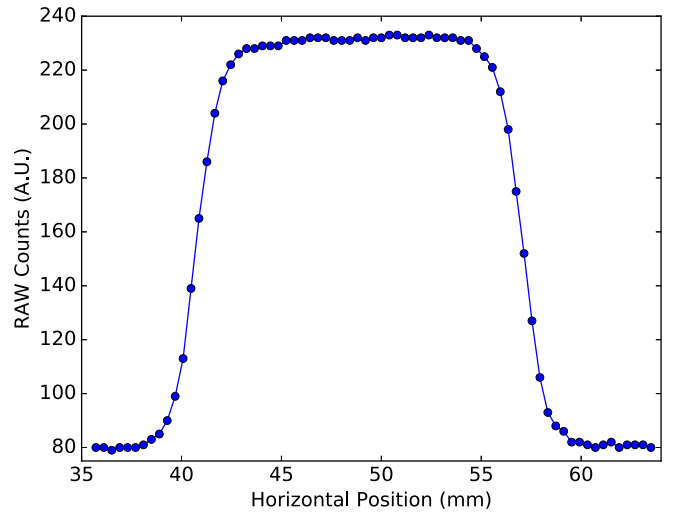


Fig. 7. Horizontal proton beam profile at a depth of 29.0 mm within the water using a 15.4 mm square collimator.

Table 1

Horizontal profile characteristics at different positions along the raw bragg peak, using a square 15.4 mm collimator width.

Depth (mm)	PW9010 (mm)	FWHM (mm)
0	1.9 ± 0.1	16.2 ± 0.1
29.0	2.6 ± 0.1	16.3 ± 0.1
33.3	3.5 ± 0.1	16.1 ± 0.1

3.5. Vertical profiles

Vertical profiles were measured, where the fiber was moved perpendicular to the beam in the direction along the scintillating fiber's axis, whilst in the horizontal center of the beam. The fiber was initially centered vertically in the beam, which was collimated with a 19 mm square collimator. This was done at depths within the water of 7.9 mm and 23.8 mm, and the results are shown in Fig. 8. The 0 mm position point actually corresponds to the fiber placed lower than the beam center, so after an initial plateau in counts where the entire fiber is being irradiated, we expect the signal to drop linearly with increasing distance, since the amount of fiber being irradiated is decreasing as it is being pulled out of the beam. The final plateau is after the fiber is no

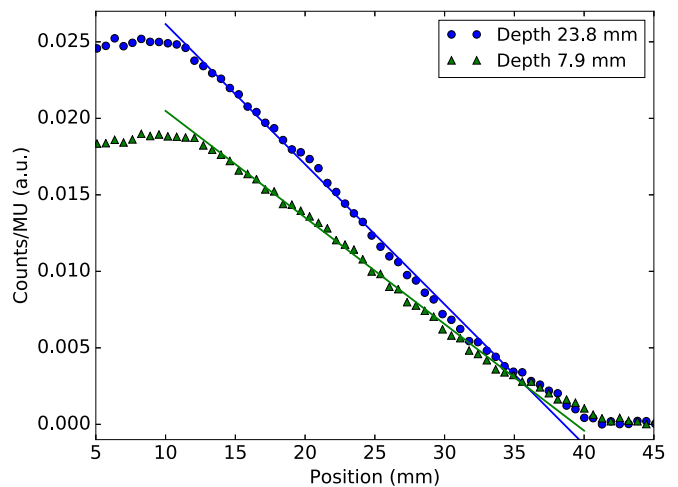


Fig. 8. Vertical scans of the fiber at the center of the beam in the horizontal direction at depths of 7.9 mm and 23.8 mm within the water box using a 19 mm square collimator.

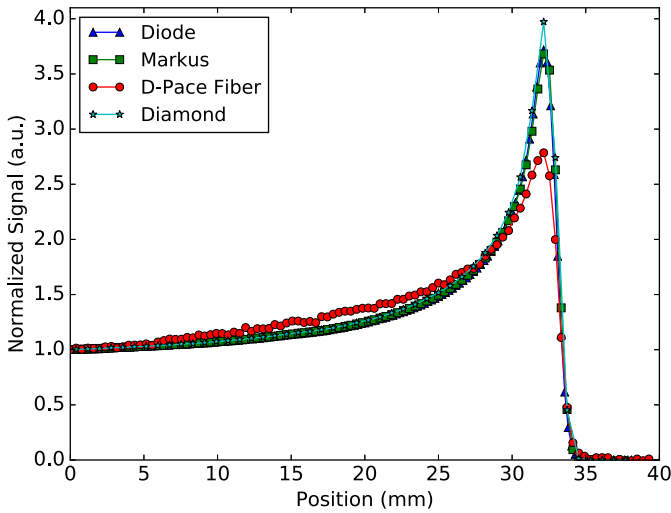


Fig. 9. Depth-dose profiles for the RBP using various dosimeters.

longer being irradiated with protons.

We see this expected linearity for both depths in the water in Fig. 8, with $R^2 > 0.99$ for each depth. Therefore, the signal from the fiber is proportional to its irradiation length regardless of depth, or independently of irradiated dose levels. The deviation at the end of the linear decrease is most likely due to protons scattering to the portion of the fiber which has been pulled out of the primary beam, generating a slightly elevated signal.

3.6. Depth profiles

We measured the signal within the water box as a function of fiber depth, essentially measuring the Raw Bragg Peak for the protons within water. This was done by putting the fiber against the edge of the box and along the center (horizontally and vertically) of the beam, and then scanning axially through further depths in water. The results are compared to reference data for other detectors in Fig. 9. The other detectors used are the PTW TN60019 Diamond Detector, BPW 34 optical diode, and the PTW Markus detectors, which are all standards in the field of radiation therapy. The profiles were shifted in position so that all signal peaks were aligned, and then normalized to the starting position of the fiber.

The peak-to-plateau ratio for the fiber, which is essentially a measure of the quenching level, is 2.79. The other diamond/diode/markus detectors have peak-to-plateau ratios of 3.97/3.72/3.68 respectively. In our previous work we tested a different Ce-doped fiber at the same beamline with the same beam energy. This fiber has a peak-to-plateau of 2.6 (Hoehr et albib_Hoehr_et_al_Girard). Therefore, the here discussed fiber displays less severe quenching.

We repeated the same experiment, but instead used the modulator wheel to create the Spread Out Bragg Peak. The result is shown in Fig. 10, which includes the results using the reference detectors discussed previously. It is clear from these measurements that the fiber has significant quenching, and that for depth dose measurements, other detectors have superior response.

Using SRIM, we interpolated the proton's stopping power due to ionization at each depth within the water for the RBP profile in order to get the signal as a function of stopping power. The signal vs interpolated stopping power for the fiber was fit to equation (1), and the result is shown in Fig. 11. We found $k_B = 2.34 \times 10^{-2} \frac{cm}{MeV}$, and $C = 5.84 \times 10^{-5} \left(\frac{cm}{MeV}\right)^2$. These are higher than what we find for typical plastic scintillators (Torrison, 2000) ($k_B \leq 2.07 \times 10^{-2} \frac{cm}{MeV}$, $C \leq 5 \times 10^{-5} \left(\frac{cm}{MeV}\right)^2$), meaning that the fiber experiences higher quenching than common plastic scintillators as well.

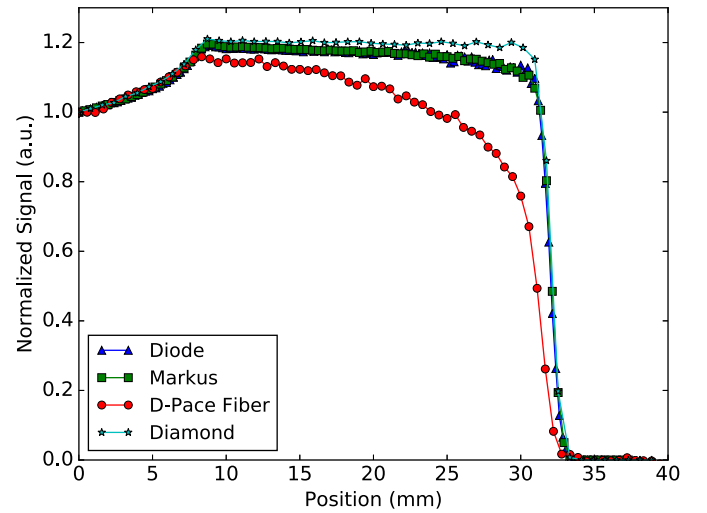


Fig. 10. Depth dose profiles for the SOBp using various dosimeters.

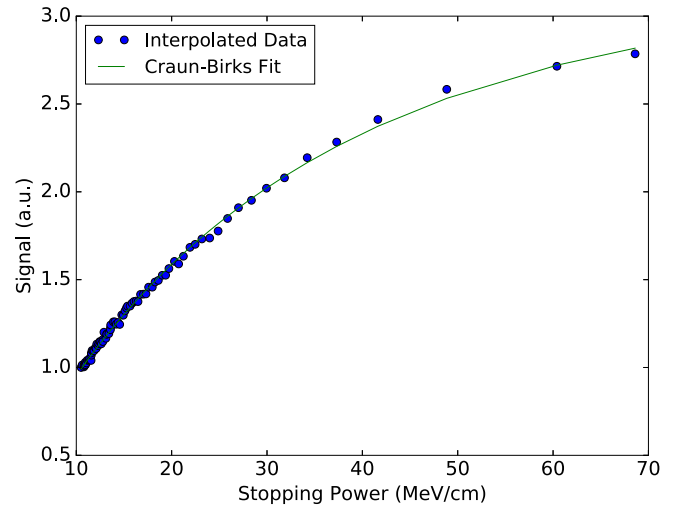


Fig. 11. D-Pace fiber signal vs interpolated stopping power for the RBP (using SRIM), with a fit to the Craun-Birks Equation. Find $k_B = 2.34 \times 10^{-2} \frac{cm}{MeV}$, and $C = 5.84 \times 10^{-5} \left(\frac{cm}{MeV}\right)^2$.

3.7. Background signal

To assess the background of the scintillator, commercial fiber, SiPM and Ortec system, the signal from the system was measured for 60 s at different positions, with and without the beam. Each position measurement was repeated three times. The system had a significant background rate without beam, but was relatively constant at different positions with $(1406 \pm 12) \times 10^{-8}$ oculombs/min. The measurement positions were at the front of the water box in the beam center, at the front of the water box outside the beam path, and in the Bragg peak position in the beam center. The background rate was 45% of the signal with beam on at the entrance of the water box, and 26% of the signal with beam on in the Bragg peak.

In proton beams, the Cerenkov signal in scintillators and the optical fiber cable is expected to be insignificant in comparison to the scintillation signal due to the energy threshold for Cerenkov production by protons (Archambault et al., 2008, Hoehr et al). To estimate how much of this background is coming from the commercial fiber instead of the scintillator, the scintillator was removed and the background measurements repeated with the commercial fiber in the same position as before. In this case, measurements with the beam on resulted in $(1421 \pm 2) \times 10^{-8}$ coulombs/min and without the beam in

$(1422 \pm 1) \times 10^{-8}$ coulombs/min, therefore no difference in background was found due to differing positions or beam status. This indicates that no additional scintillation light was induced in the commercial fiber due to the proton beam. This is consistent with our previous measurement with a different Ce-doped fiber (Hoehr et al).

4. Conclusion

The Ce-doped silica fiber used by D-Pace in their UniBEaM25 beam profiler system was shown to be reproducible in signal within 1.15%, and produce a signal which is linear to the irradiated dose and its irradiated length independent of the average proton energy incident on the fiber. These characteristics, along with its very small size, allow it to be effective for profiling charged particle beams. However, it was also found to have a strong quenching attribute, with a peak-to-plateau signal ratio of 2.79 for the proton raw bragg peak profile. Most standards in the dosimetric field expect a value of 3.7 or higher for this therapeutic proton beam, and so for the fiber to be effective at measuring irradiated dose, the signal would need to be calibrated to a characteristic quenching curve (via the Craun-Birks equation) of the fiber.

Acknowledgment

Funding for this work was provided by National Sciences and Engineering Research Council of Canada (EGP 507425-2016). TRIUMF receives federal funding via a contribution agreement with the National Research Council of Canada.

On behalf of D-Pace, the authors gratefully acknowledge the financial contributions of the Canadian government SRED program and NRC program (IRAP 825062), and Buckley Systems Ltd. In addition, the authors wish to express their appreciation to the AEC-LHEP, University of Bern for their ongoing support with the commercialization of UniBEaM, and to the Department of Material Science, University of Milano-Bicocca for their expertise in scintillating optical fibers.

References

- Archambault, L., Polf, J., Beaulieu, L., Beddar, S., 2008. Characterizing the response of miniature scintillation detectors when irradiated with proton beams. *Phys. Med. Biol.* 53, 18651876.
- Braccini, S., Ereditato, A., Giacoppo, F., Kreslo, I., Nesteruk, K.P., Nirkko, M., Weber, M., Scamporrì, P., Neff, M., Pilz, S., Romano, V., 2012. A beam monitor detector based on doped silica and optical fibres. *J. Instrum.* 7 (02), T02001. <http://stacks.iop.org/1748-0221/7/i=02/a=T02001>.
- C. Hoehr, A. Morana, O. Duhamel, B. Capoen, M. Trinczek, C. Duzenli, P. Paillet, H. E. Hamzaoui, M. Bouazaoui, G. Bouwmans, Y. Ouerdane, A. Boukenter, S. Girard, Potential of novel optical fibers for proton therapy dosimetry, IEEE MIC Conference Record Submitted.
- G. F. Knoll, *Radiation Detection and Measurement*, Wiley..
- Mones, E., Veronese, I., Moretti, F., Fasoli, M., Loi, G., Negri, E., Brambilla, M., Chiodini, N., Brambilla, G., Vedda, A., 2006. Feasibility study for the use of ce3+-doped optical fibres in radiotherapy. *Nucl. Instrum. Methods Phys. Res. Sect. A Accel. Spectrom. Detect. Assoc. Equip.* 562 (1), 449–455. <http://doi.org/10.1016/j.nima.2006.02.003> <http://www.sciencedirect.com/science/article/pii/S0168900206002348>.
- Mones, E., Veronese, I., Vedda, A., Loi, G., Fasoli, M., Moretti, F., Chiodini, N., Cannillo, B., Brambilla, M., 2008. Ce-doped optical fibre as radioluminescent dosimeter in radiotherapy. *Radiat. Meas.* 43 (26), 888–892. proceedings of the 15th Solid State Dosimetry (SSD15). <http://doi.org/10.1016/j.radmeas.2008.01.031>. <http://www.sciencedirect.com/science/article/pii/S1350448708000450>.
- Torrì, L., 2000. Plastic scintillator investigations for relative dosimetry in proton-therapy. *Nucl. Instrum. Methods Phys. Res. Sect. B Beam Interact. Mater. Atoms* 170 (3), 523–530. [https://doi.org/10.1016/S0168-583X\(00\)00237-8](https://doi.org/10.1016/S0168-583X(00)00237-8) <http://www.sciencedirect.com/science/article/pii/S0168583X00002378>.
- UNIBEAM25, BEAM PROFILER SYSTEM User Manual.
- Vedda, A., Chiodini, N., Martino, D.D., Fasoli, M., Keffer, S., Lauria, A., Martini, M., Moretti, F., Spinolo, G., Nikl, M., Solovieva, N., Brambilla, G., 2004. Ce3+-doped fibers for remote radiation dosimetry. *Appl. Phys. Lett.* 85 (26), 6356–6358. <http://dx.doi.org/10.1063/1.1840127>. <https://doi.org/10.1063/1.1840127>.
- Veronese, I., Cantone, M., Chiodini, N., Coray, A., Fasoli, M., Lomax, A., Mones, E., Moretti, F., Vedda, A., 2010. Feasibility study for the use of cerium-doped silica fibres in proton therapy. *Radiat. Meas.* 45 (36), 635–639. proceedings of the 7th European Conference on Luminescent Detectors and Transformers of Ionizing Radiation (LUMDETR 2009). <http://doi.org/10.1016/j.radmeas.2009.10.100>. <http://www.sciencedirect.com/science/article/pii/S1350448709002765>.
- Yanagida, T., 2013. Study of rare-earth-doped scintillators. *Opt. Mater.* 35 (11), 1987–1992. photoluminescence in Rare Earths: Photonic Materials and Devices - Selected papers from PRE'12 Conference. <https://doi.org/10.1016/j.optmat.2012.11.002>. <http://www.sciencedirect.com/science/article/pii/S0925346712004715>.
- J. F. Ziegler, *Interactions of Ions with Matter*. <http://www.srim.org/>.